

Amorphous Solid Model of Vectorial Hopfield Neural Networks

Filippo Gallavotti* and Alessio Zaccone†

Department of Physics “A. Pontremoli”, University of Milan, via Celoria 16, 20133 Milan, Italy

We introduce a three-dimensional vector Hopfield model where each neuron is a unit vector on S^2 and synaptic weights are 3×3 blocks built by a vectorial Hebbian rule, analogous to the Hessian of amorphous solids. The resulting rigid energy landscape strongly stabilizes stored patterns. Simulations and spectral analysis show that the critical storage ratio grows roughly linearly with connectivity and enters a high-connectivity regime with enhanced capacity, a persistent spectral gap, and enlarged basins of attraction, yielding robust associative memory.

The Hopfield model [1] is a cornerstone of associative memory in neural networks and artificial intelligence [2]. In its classical formulation, N binary neurons $s_i \in \{-1, +1\}$ evolve according to symmetric interactions W_{ij} defined by the Hebbian rule from stored patterns. The dynamics minimizes $E = -\frac{1}{2} \sum_{ij} W_{ij} s_i s_j$, leading to pattern retrieval via convergence to energy minima. Connections between neural network models and disordered materials have been explored in spin glasses [3–5], jammed packings [6, 7], random resistor and memristive networks [8], and elastic networks [9]. Recent work has emphasized the relation between the “cost landscape” and the physical landscape encoded by the cost Hessian and physical Hessian, respectively [10].

Neural networks and amorphous solids share structural similarities in their interaction matrices and in the emergence of multiple metastable states. In amorphous solids the Hessian describing elastic interactions exhibits a random block structure analogous to weight matrices in neural networks with vectorial degrees of freedom.

Motivated by this analogy, we introduce a multi-dimensional extension of the Hopfield model. Each neuron is a unit vector $\mathbf{s}_i \in \mathbb{R}^3$, and interactions are built through outer products following a vectorial Hebbian rule. This uses random block matrices previously introduced for amorphous solids [11, 12] and only recently adopted in neural network theory [5].

The vectorial extension is relevant to systems with orientational degrees of freedom, such as liquid crystals, polymeric glasses, biological networks such as the cytoskeleton, and enables systematic comparison with classical binary Hopfield networks [13]. We start by reviewing the binary Hopfield model.

We consider 3D networks of N nodes (neurons) connected by 3D vectors (“bonds” or synapses) as in Fig. 1. In the amorphous solid analogy, the connections are springs with spring constant κ [14–16].

The binary Hopfield model consists of N neurons with $s_i \in \{-1, +1\}$. To store P patterns $\{\boldsymbol{\xi}^\mu\}_{\mu=1}^P$ with $\boldsymbol{\xi}^\mu = (\xi_1^\mu, \dots, \xi_N^\mu)$ and $\xi_i^\mu \in \{-1, +1\}$, the weight matrix is

$$W_{ij} = \frac{1}{N} \sum_{\mu=1}^P \xi_i^\mu \xi_j^\mu \quad (1)$$

with $W_{ii} = 0$ and $W_{ij} = W_{ji}$. The dynamics follows

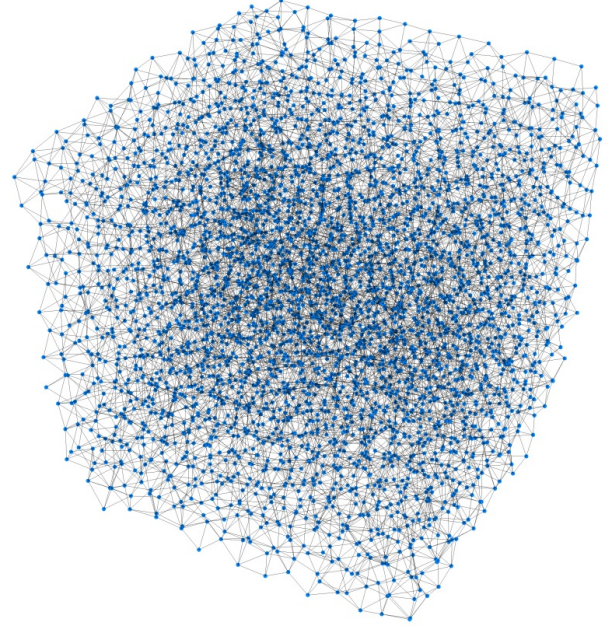


FIG. 1: Rendering of a 3D network of N nodes with average coordination number $Z = 7$ and nearly uniform orientation distribution.

asynchronous updates $s_i \leftarrow \text{sign}(\sum_j W_{ij} s_j)$, which minimize $E = -\frac{1}{2} \sum_{ij} W_{ij} s_i s_j$. Neuron i updates according to its total input, with $\Delta E \leq 0$, and pattern retrieval occurs when the system converges from partial or noisy initial states.

In the vectorial model, each neuron is a unit vector $\mathbf{s}_i \in \mathbb{R}^3$ with $|\mathbf{s}_i| = 1$. We store P patterns $\{\boldsymbol{\xi}^\mu\}_{\mu=1}^P$, where each pattern is a set of N random unit vectors on S^2 :

$$\boldsymbol{\xi}^\mu = (\xi_1^\mu, \dots, \xi_N^\mu), \quad |\xi_i^\mu| = 1. \quad (2)$$

The weight matrix is defined via a vectorial Hebbian rule using outer products:

$$\mathbf{W}_{ij} = \frac{1}{N} \sum_{\mu=1}^P \boldsymbol{\xi}_i^\mu \otimes \boldsymbol{\xi}_j^\mu \quad (3)$$

where \otimes denotes the outer product, yielding 3×3 blocks

\mathbf{W}_{ij} . The full matrix \mathbf{W} is $3N \times 3N$ with block structure [12].

This parallels the Hessian in amorphous solids [11]. For elastic interactions between particles at positions \mathbf{r}_i ,

$$H_{ij}^{\alpha\beta} = \kappa_{ij} n_{ij}^{\alpha} n_{ij}^{\beta} \quad (4)$$

with spring constant κ_{ij} and bond unit vector

$$\mathbf{n}_{ij} = (\sin \theta \cos \phi, \sin \theta \sin \phi, \cos \theta), \quad (5)$$

where $\alpha, \beta = \{x, y, z\}$. Self-interactions are ignored. The structure matches Eq. (3), with stored patterns playing the role of bond directions.

The energy is

$$E(\mathbf{s}) = -\frac{1}{2} \sum_{i,j=1}^N \mathbf{s}_i^T \mathbf{W}_{ij} \mathbf{s}_j \quad (6)$$

and the dynamics preserves $|\mathbf{s}_i| = 1$ by normalizing the local field $\mathbf{h}_i = \sum_{j \neq i} \mathbf{W}_{ij} \mathbf{s}_j$ via $\mathbf{s}_i^{\text{new}} = \mathbf{h}_i / |\mathbf{h}_i|$.

Simulations show reliable retrieval: from random initial configurations, dynamics converges to stored patterns (or complements) within ~ 30 asynchronous updates.

To construct the synaptic matrix, we use a pseudo-inverse learning rule instead of standard Hebbian learning. The classical rule is optimal only for mutually orthogonal patterns, which is not generic at finite P/N . To enforce exact retrieval, we adopt a pseudo-inverse generalization. Defining the pattern matrix $\Xi = [\xi^{(1)} \xi^{(2)} \dots \xi^{(P)}]$ of size $3N \times P$, the Gram matrix of overlaps is

$$G_{\mu\nu} = \frac{1}{N} \sum_{i=1}^N \xi_i^{\mu} \cdot \xi_i^{\nu}, \quad (7)$$

and its inverse G^{-1} defines the pseudo-inverse operator

$$W = \frac{1}{N} \sum_{\mu, \nu=1}^P \Xi_{\mu} (G^{-1})_{\mu\nu} \Xi_{\nu}^{\top}, \quad (8)$$

which satisfies $W\Xi = \Xi$, so each stored pattern is an exact eigenvector of W with eigenvalue 1. This guarantees perfect recall of all training patterns in the fully connected case and provides a natural extension of the classical formulation to correlated patterns.

We next study how memory capacity depends on network connectivity. We introduce a Z -connected topology, where each neuron is symmetrically coupled to its $Z/2$ nearest neighbours on either side along a circular ring. The coordination number Z interpolates between fully connected ($Z = N - 1$) and sparse ($Z \ll N$) networks. The adjacency matrix C_{ij} satisfies

$$C_{ij} = \begin{cases} 1, & \text{if } j \in \text{neigh}(i) \text{ or } i \in \text{neigh}(j), \\ 0, & \text{otherwise.} \end{cases}$$

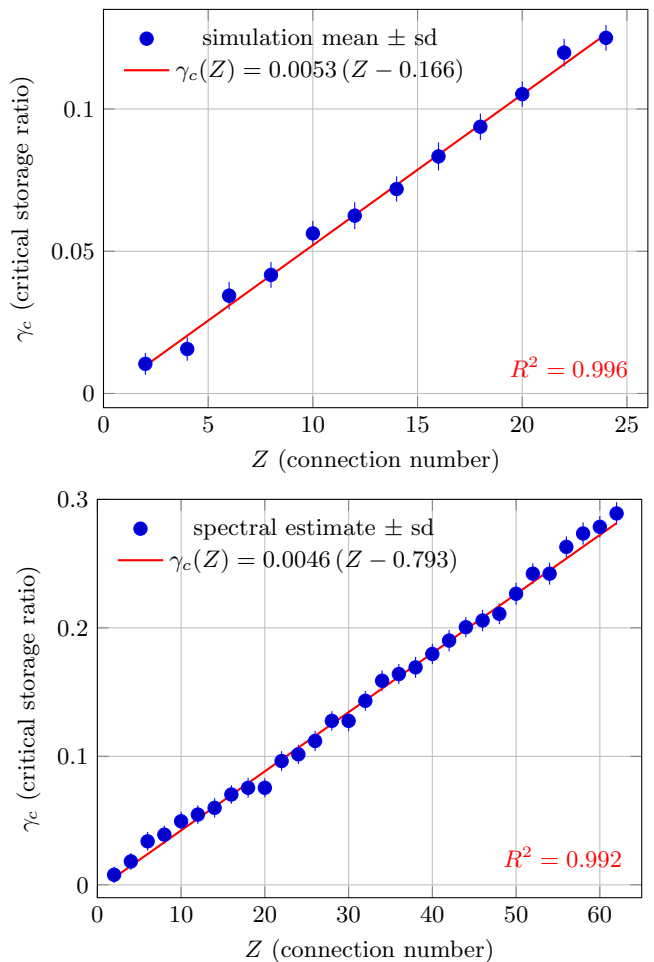


FIG. 2: Critical storage capacity versus connectivity.

Top figure: Dynamical estimate of γ_c with standard-deviation error bars across 5 replicas. Bottom figure: Spectral estimate from the vanishing smallest eigenvalue of the Hessian at each attractor. Both panels show an approximately linear dependence of γ_c on Z with closely matching slopes.

Synaptic weights are built locally by solving, for each neuron i , a regularized linear system enforcing consistency between target outputs ξ_i^{μ} and inputs from neighbours ξ_j^{μ} in all stored patterns. With \mathcal{N}_i the neighbour set of i , the local matrices $\{W_{ij}\}_{j \in \mathcal{N}_i}$ satisfy

$$\sum_{j \in \mathcal{N}_i} W_{ij} \xi_j^{\mu} \simeq \xi_i^{\mu}, \quad \forall \mu = 1, \dots, P,$$

via the ridge-regularized least-squares solution

$$W_i = (X_i X_i^{\top} + \lambda I)^{-1} X_i Y_i^{\top},$$

where X_i collects neighbour states and Y_i the target states for neuron i . The parameter λ ensures numerical stability and controls smoothness. This local pseudo-inverse generalizes the fully connected rule to sparse graphs while encoding topology.

Figure 2 shows that, for moderate connectivity, the critical storage capacity γ_c increases approximately linearly with Z . A linear regression (for $N = 64$ neurons, $T = 500$ trials, and $L = 1000$ maximum asynchronous updates) yields

$$\gamma_c(Z) = 0.0053(Z - 0.17), \quad R^2 = 0.996.$$

Each additional connection reinforces the effective local field, thereby enlarging basins of attraction: increasing Z stiffens the associative energy landscape, deepening and separating minima corresponding to memorized states. The nearly linear growth reflects a mean-field balance between stabilizing recurrent couplings and destabilizing cross-talk.

To corroborate this picture, we performed a spectral analysis of the Hessian at each attractor, identifying γ_c as the point where the smallest eigenvalue λ_{\min} vanishes, i.e. the loss of local stability. The resulting relation

$$\gamma_c(Z) = 0.0046(Z - 0.79), \quad R^2 = 0.992,$$

is in excellent agreement with the dynamical estimate. The consistency between dynamical and spectral approaches shows that the transition from stable to unstable retrieval corresponds to a spectral softening of the Hessian, analogous to the vanishing lowest vibrational mode at jamming. Thus the linear dependence of γ_c on Z supports an interpretation of associative-memory stability as an emergent rigidity phenomenon in a high-dimensional landscape.

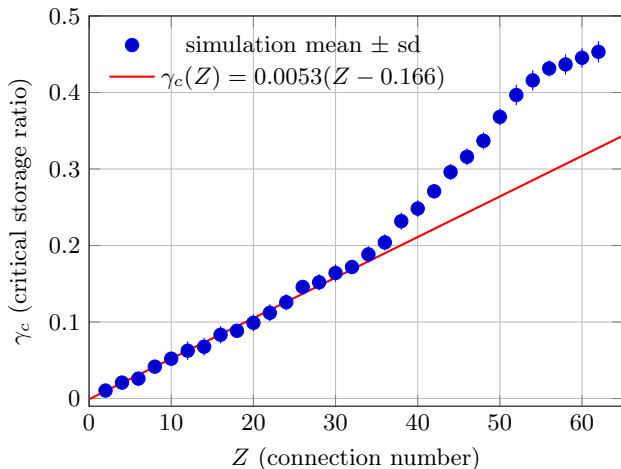


FIG. 3: High-connectivity regime of critical storage capacity. Symbols: spectral estimate of γ_c (mean \pm sd) versus Z . Red line: linear trend $\gamma_c(Z) = 0.0053(Z - 0.166)$ obtained at moderate Z (cf. Fig. 2). The systematic upward deviation at large Z signals a crossover to an enhanced-capacity regime where γ_c exceeds the extrapolated low- Z prediction.

Beyond the moderate-connectivity regime of Fig. 2, Fig. 3 shows a crossover at large Z where γ_c rises faster

than the low- Z linear trend $\gamma_c(Z) = 0.0053(Z - 0.166)$. The deviation is systematic and becomes pronounced for $Z \gtrsim 30$, indicating an enhanced-capacity regime. Increased local redundancy and orientational constraints in the block-structured operator strengthen effective fields and reduce cross-talk, effectively “rigidifying” the associative landscape. This is consistent with the spectral picture, where pattern modes remain separated from the bulk, indicating stronger attractor stability as connectivity increases. While finite-size effects cannot be completely excluded, the monotonic upward curvature with Z points to a genuine connectivity-driven gain beyond the linear mean-field regime.

We next examine how pattern orientation distributions affect memory capacity by generating patterns with random orientations for \mathbf{n}_{ij} . Because \mathbf{n}_{ij} is parametrized by $\{\theta, \phi\}$ [Eq. (5)], both θ and ϕ are drawn from Gaussian distributions normalized over $[0, \pi]$ and $[0, 2\pi]$, respectively. In the limit $\sigma \rightarrow \infty$, the orientation distribution in solid angle is uniform, with probability $1/4\pi$ [11, 17].

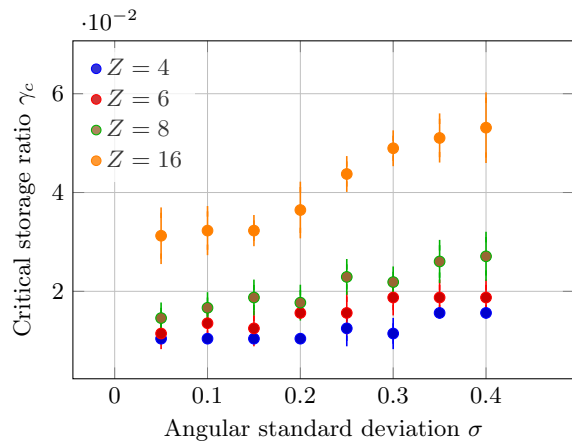


FIG. 4: Critical storage load $\gamma_c = P_c/(Nd)$ versus angular standard deviation σ of the pattern-orientation distribution, for different connectivities Z . Higher connectivity yields larger capacity for all levels of orientational disorder, with γ_c increasing with σ . Error bars: standard deviation across 5 replicas.

The critical coupling γ_c depends on both orientational disorder σ and connectivity Z . As shown in Fig. 4, γ_c increases with σ for each Z , with fluctuations due to finite sampling of P_{critical} . Networks with higher connectivity consistently achieve greater memory capacity: for $Z = 4$, γ_c ranges from 0.0104 to 0.0156, while for $Z = 16$ it increases from 0.0313 to 0.0531 over the same σ range. Thus denser networks support higher baseline capacity and gain more from orientational disorder.

The monotonic increase of γ_c with σ suggests that more diverse orientations create a more robust memory landscape, reducing interference between stored patterns via orientation-based differentiation. This enhanced stability

requires stronger synaptic coupling, as reflected in higher γ_c values. The variations of $\gamma_c(\sigma)$ across different Z indicate that connectivity controls how orientational disorder affects pattern stability: sparse networks require a minimum orientational diversity to overcome limited connectivity, whereas dense networks exploit orientation diversity effectively over the full parameter range.

The vectorial Hopfield model generates energy landscapes with multiple local minima corresponding to stored patterns. We quantify pattern stability via the energy difference between stored and random configurations. For $N = 25$ and $\gamma = 0.1$, stored patterns have mean energies about 7 units lower than random states, ensuring robust retrieval against initialization noise. The energy function given by Eq. (6) naturally creates this hierarchy through the outer-product construction of \mathbf{W} . The energy gap decreases as γ approaches γ_c , paralleling metastable hierarchies in glass-forming systems [18–20].

The eigenvalue spectrum of W_{ij} [Eq. (1)] characterizes computational properties at different pattern densities (see Fig. 7 in the End Matter). For low density ($\gamma = 0.05$), the spectrum shows isolated pattern eigenvalues and a bulk near zero. For intermediate density ($\gamma = 0.1$ – 0.2), a bulk develops with pattern eigenvalues as outliers. For high density ($\gamma = 0.5$), the spectrum approaches random-matrix behavior. The evolution of spectral density with γ reflects a crossover from a memory-dominated to a noise-dominated regime; γ_c corresponds to the merging of pattern eigenvalues with the bulk and the loss of discriminability.

Convergence properties depend on initialization and pattern density. The convergence time scales logarithmically with system size N for successful retrievals, while basin size decreases approximately exponentially as γ approaches γ_c , and basin boundaries become more complex. The unit-vector constraint produces dynamics on the product manifold $S^2 \times S^2 \times \dots \times S^2$, preserving pattern structure but adding geometric complexity. The update rule

$$\mathbf{s}_i^{(t+1)} = \frac{\mathbf{h}_i^{(t)}}{|\mathbf{h}_i^{(t)}|}, \quad \mathbf{h}_i^{(t)} = \sum_{j \neq i} \mathbf{W}_{ij} \mathbf{s}_j^{(t)} \quad (9)$$

ensures convergence to fixed points while enforcing the spherical constraint.

The block-structured matrix \mathbf{W} encodes orientational correlations through its 3×3 blocks \mathbf{W}_{ij} . We characterize them via (i) the Frobenius norm $|\mathbf{W}_{ij}|_F$, measuring interaction strength, and (ii) the anisotropy ratio $\lambda_{\max}/\lambda_{\min}$ of $\mathbf{W}_{ij}^T \mathbf{W}_{ij}$, measuring directional bias. For typical systems we find $\langle |\mathbf{W}_{ij}|_F \rangle \approx 0.02$ and $\langle \lambda_{\max}/\lambda_{\min} \rangle \approx 15$, indicating strongly directional interactions due to the vectorial nature of stored patterns. This correlation structure produces emergent organization in \mathbf{W} , with stronger correlations between blocks associated with patterns of similar orientation.

The vectorial Hopfield model introduced here extends associative memory beyond binary states by assigning to each neuron a unit vector on S^2 and implementing block-structured couplings analogous to the Hessian of disordered solids. This construction generates a rigid energy landscape with well-separated minima associated with the stored patterns and monotonic Lyapunov descent under the spherical constraint.

Our results show a clear performance gain over the classical binary Hopfield network. For moderate connectivity, the critical storage ratio γ_c grows approximately linearly with Z , with dynamical and spectral estimates in close agreement [Fig. 2]. The high-connectivity data [Fig. 3] reveal a further enhancement: for large Z , γ_c systematically exceeds the extrapolated low- Z linear trend, indicating a crossover to an enhanced-capacity regime. This behaviour is consistent with a connectivity-driven “rigidification” of the associative landscape, whereby additional block couplings increase local redundancy, strengthen effective fields, and reduce cross-talk.

Spectral analysis supports this interpretation: pattern modes remain well separated from the bulk over an extended range of loads, and the associated basins of attraction are larger and more stable, enabling robust retrieval even from strongly corrupted initial conditions. These features have no analogue in the standard Hopfield model at comparable load, underscoring the advantage of vectorial degrees of freedom and amorphous-solid-inspired architecture.

Promising extensions include nonlinear learning rules, sparse or hierarchical connectivities that retain the high- Z advantage, and higher-dimensional state manifolds [21]. Overall, the vectorial Hopfield framework provides a compact, high-capacity associative memory that markedly outperforms the classical binary model in the moderate- to high-connectivity regime.

ACKNOWLEDGMENTS

AZ gratefully acknowledges funding from the European Union through Horizon Europe ERC Grant number: 101043968 “Multimech”. During the preparation of this work we became aware of similar observations in a vectorial spin-glass model [5].

END MATTER

This appendix collects the numerical diagnostics supporting the results presented in the main text. We report: (i) direct evidence of Lyapunov convergence; (ii) the spectral softening of the Hessian leading to the critical load; (iii) the evolution of the weight-matrix spectrum with increasing pattern density; (iv) quantitative energy separation between memory and spurious minima.

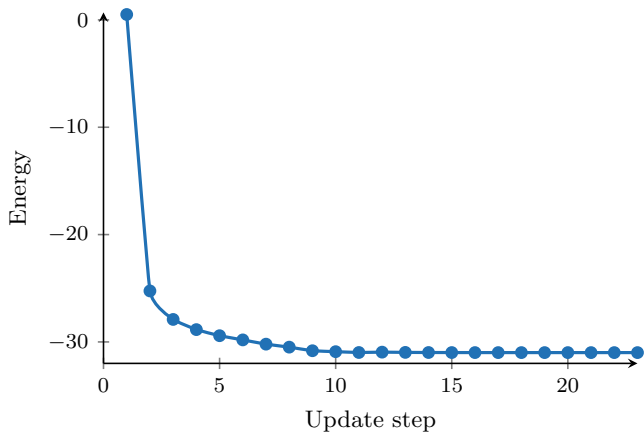


FIG. 5: Monotonic decay of the Lyapunov energy $E(t)$ during synchronous updates for $N = 25$, $d = 3$, $P = 5$. The system converges rapidly to the minimum associated with the retrieved memory.

The loss of stability of stored patterns is captured by the smallest eigenvalue λ_{\min} of the Hessian. The curve in Fig. 6 shows the softening and zero-crossing of λ_{\min} as the load γ approaches the critical value.

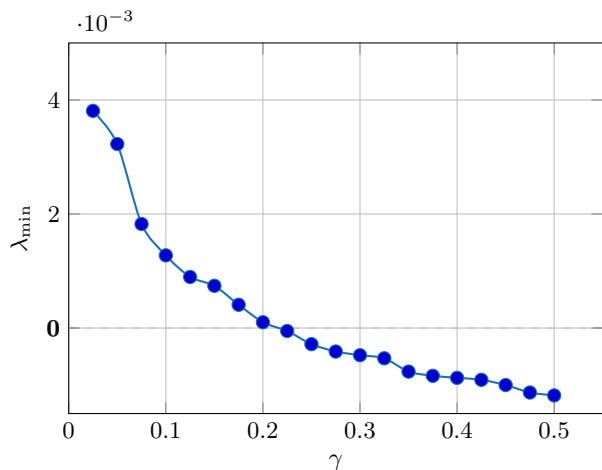


FIG. 6: Minimum eigenvalue of the Hessian for a fully connected network ($Z = 63$). The zero-crossing at $\gamma_c^{\text{spec}} \simeq 0.21$ marks the onset of instability of the memory attractors.

Figure 7 displays the spectral density of the weight matrix W for increasing pattern loads. As γ grows, isolated outliers merge with the bulk and the spectrum broadens into a continuous band, consistent with the breakdown of retrieval capacity.

Finally, the table below summarises the energy separation between stored patterns and spurious minima for three representative load levels. Energies are obtained

from 300 random initialisations for each value of γ/γ_c .

γ/γ_c	E_{\min}^{mem}	E_{\min}^{SP}	Gap ΔE
0.1	-30.397	—	—
0.3	-27.681	-27.199	+0.482
0.7	-24.952	-24.884	+0.068

TABLE I: Energies of stored memories and deepest spurious minima. Large gaps at low load reflect clean memory dominance; near capacity the gap collapses, consistent with interference-driven instability.

* filippo.gallavotti@studenti.unimi.it

† alessio.zaccane@unimi.it

- [1] J. J. Hopfield, Proceedings of the National Academy of Sciences **79**, 2554 (1982), <https://www.pnas.org/doi/pdf/10.1073/pnas.79.8.2554>.
- [2] L. Meshulam and W. Bialek, Rev. Mod. Phys. **97**, 045002 (2025).
- [3] D. J. Amit, H. Gutfreund, and H. Sompolinsky, Phys. Rev. A **32**, 1007 (1985).
- [4] M. Baity-Jesi, L. Sagun, M. Geiger, S. Spigler, G. B. Arous, C. Cammarota, Y. LeCun, M. Wyart, and G. Biroli, in *Proceedings of the 35th International Conference on Machine Learning*, Proceedings of Machine Learning Research, Vol. 80, edited by J. Dy and A. Krause (PMLR, 2018) pp. 314–323.
- [5] F. Nicoletti, F. D’Amico, and M. Negri, “Statistical mechanics of vector hopfield network near and above saturation,” (2025), arXiv:2507.02586 [cond-mat.dis-nn].
- [6] M. Geiger, S. Spigler, S. d’Ascoli, L. Sagun, M. Baity-Jesi, G. Biroli, and M. Wyart, Phys. Rev. E **100**, 012115 (2019).
- [7] G. Zhang, D. J. Heeger, and S. Martiniani, “Contrastive self-supervised learning as neural manifold packing,” (2025), arXiv:2506.13717 [cs.LG].
- [8] S. G. Hu, Y. Liu, Z. Liu, T. P. Chen, J. J. Wang, Q. Yu, L. J. Deng, Y. Yin, and S. Hosaka, Nature Communications **6**, 7522 (2015).
- [9] L. E. Altman, M. Stern, A. J. Liu, and D. J. Durian, Phys. Rev. Appl. **22**, 024053 (2024).
- [10] M. Stern, M. Guzman, F. Martins, A. J. Liu, and V. Balasubramanian, Phys. Rev. Lett. **134**, 147402 (2025).
- [11] A. Zaccane and E. Scossa-Romano, Physical Review B **83**, 184205 (2011).
- [12] G. M. Cicuta, J. Krausser, R. Milkus, and A. Zaccane, Phys. Rev. E **97**, 032113 (2018).
- [13] J. A. Hertz, A. S. Krogh, and R. G. Palmer, *Introduction to the Theory of Neural Computation*, Santa Fe Institute Studies in the Sciences of Complexity, Vol. 1 (Addison-Wesley, Reading, MA, 1991) p. 327.
- [14] R. Milkus and A. Zaccane, Phys. Rev. B **93**, 094204 (2016).
- [15] R. Milkus and A. Zaccane, Phys. Rev. E **95**, 023001 (2017).
- [16] A. Zaccane, *Theory of Disordered Solids* (Springer, Cham, 2023).

- [17] A. Zaccane, J. R. Blundell, and E. M. Terentjev, Phys. Rev. B **84**, 174119 (2011).
- [18] G. Biroli and J. Kurchan, Phys. Rev. E **64**, 016101 (2001).
- [19] D. Han, D. Wei, J. Yang, H.-L. Li, M.-Q. Jiang, Y.-J. Wang, L.-H. Dai, and A. Zaccane, Phys. Rev. B **101**, 014113 (2020).
- [20] P. Charbonneau, J. Kurchan, G. Parisi, P. Urbani, and F. Zamponi, Nature Communications **5**, 3725 (2014).
- [21] D. Krotov and J. Hopfield, “Large associative memory problem in neurobiology and machine learning,” (2021), arXiv:2008.06996 [q-bio.NC].

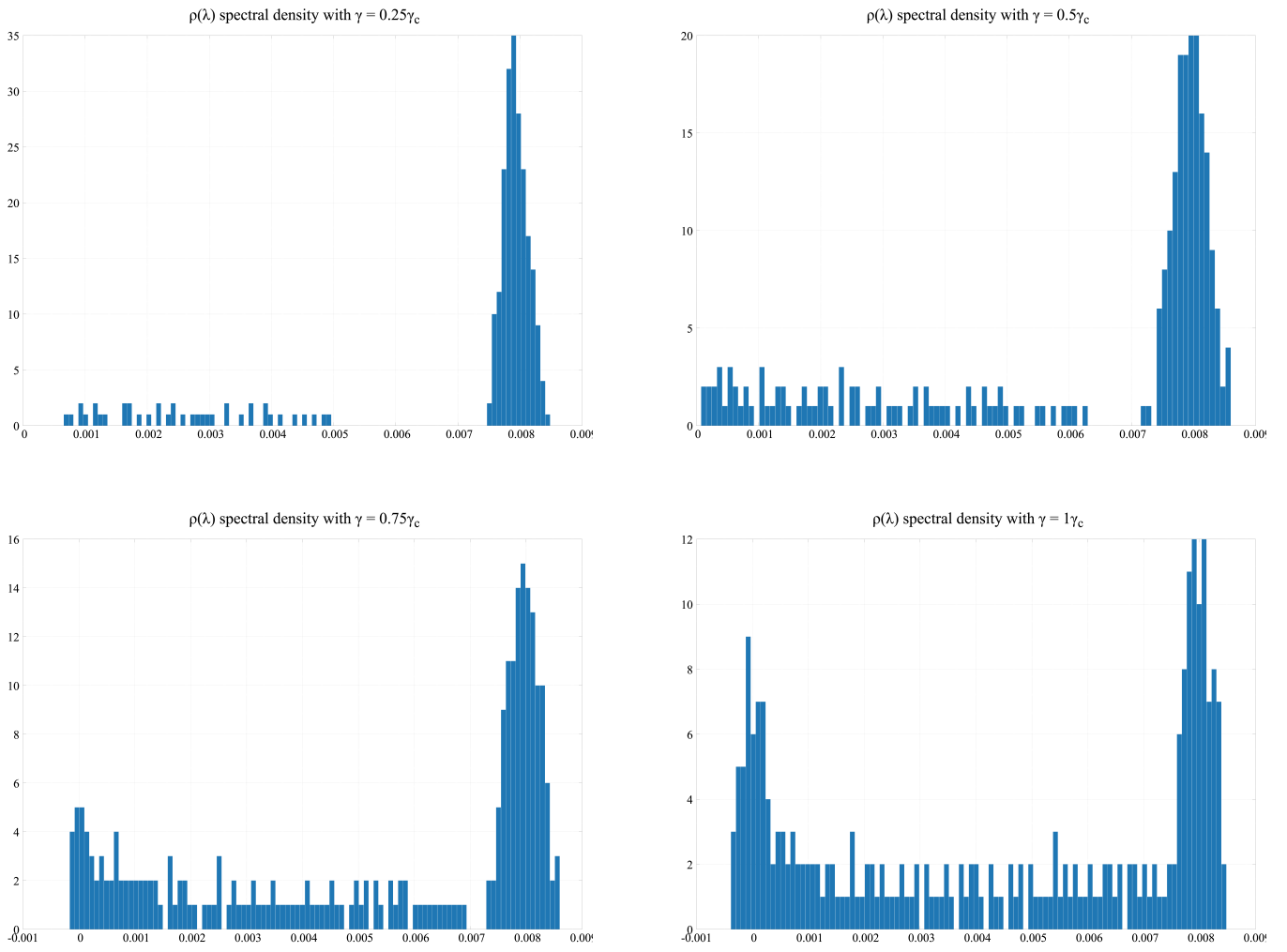


FIG. 7: Evolution of the spectral density $\rho(\lambda)$ of the weight matrix with increasing pattern load γ . Low loads (top left) exhibit isolated pattern eigenvalues; intermediate loads develop a broadened bulk; high loads (bottom right) show a continuous spectrum approaching random-matrix form.